Biosensors and Bioelectronics 65 (2015) 382–389

Contents lists available at ScienceDirect

Biosensors and Bioelectronics

journal homepage: www.elsevier.com/locate/bios

Amplified and selective detection of manganese peroxidase genes based on enzyme-scaffolded-gold nanoclusters and mesoporous carbon nitride

Yaoyu Zhou [a,b], Lin Tang [a,b,*], Guangming Zeng [a,b,*], Jun Chen [a,b], Jiajia Wang [a,b], Changzheng Fan [a,b], Guide Yang [a,b], Yi Zhang [a,b], Xia Xie [a,b]

[a] College of Environmental Science and Engineering, Hunan University, Changsha 410082, Hunan, PR China
[b] Key Laboratory of Environmental Biology and Pollution Control (Hunan University), Ministry of Education, Changsha 410082, Hunan, PR China

ARTICLE INFO

Article history:
Received 21 August 2014
Received in revised form
23 October 2014
Accepted 27 October 2014
Available online 31 October 2014

Keywords:
Mesoporous carbon nitride
Enzyme
Gold nanoclusters
Signal amplification
Biosensor

ABSTRACT

This work has demonstrated an amplified and selective detection platform using enzyme-scaffolded-gold nanoclusters as signal label, coupling with mesoporous carbon nitride (MCN) and gold nanoparticles (GNPs) modified glassy carbon electrode (GCE). Streptavidin-horseradish peroxidase (SA-HRP) has been integrated with gold nanoclusters (GNCs) as scaffold using a simple, fast and non-toxic method. The mechanisms of enzymatic amplification, redox cycling and signal amplification by this biosensor were discussed in detail. GNCs might perform important roles as electrocatalyst as well as electron transducer in these processes. The concentrations of reagents and the reaction times of these reagents were optimized to improve the analytical performances. Under the optimized condition, the signal response to enzyme-scaffolded-gold nanoclusters catalyzed reaction was linearly related to the natural logarithm of the target nucleic acid concentration in the range from 10^{-17} M to 10^{-9} M with a correlation coefficient of 0.9946, and the detection limit was 8.0×10^{-18} M (S/N=3). Besides, synthesized oligonucleotide as well as *Phanerochaete chrysosporium MnP* fragments amplified using polymerase chain reaction and digested by restriction endonucleases were tested. Furthermore, this biosensor exhibited good precision, stability, sensitivity, and selectivity, and discriminated satisfactorily against mismatched nucleic acid samples of similar lengths.

1. Introduction

Enzyme-based DNA sensors have received particular attention due to their fast response, remarkably high sensitivity, good selectivity and strong operability (Gao et al., 2011; Zhuo et al., 2014; Liu et al., 2008). Compared with conventional DNA measurement methods (Ju et al., 2003; Ye et al., 2003; Munge et al., 2005; Wang et al., 2008), they need lower operating costs and relatively simpler equipments and operation steps, while how to improve signal amplification has become the focus in applying to low-abundant DNA detection. In fact, sensitivity of enzyme-based electrochemical DNA biosensors mainly depends on three factors: the construction of electron transfer layers, the number and the geometry of immobilized signal probes (Lubin et al., 2009; Domínguez et al., 2004; Liu et al., 2005), and the properties of enzyme. To date, most of the studies regarding sensor sensitivity focused on the former two, such as using gold (Song et al., 2009), silver (Taton et al., 2000) and carbon (Nam et al., 2003) based nanomaterials for signal amplification, or reduced graphene oxide (Dong et al., 2012), magnetic nanoparticle (Zhang et al., 2013) as carriers with enzymatic cycle, increasing the linked oligonucleotide number per enzyme molecule (Domínguez et al., 2004), and applying a "stem–loop" DNA probe dually labeled with biotin and digoxigenin for stablizing the enzyme immobilization (Liu et al., 2008).

As enzyme is the predominant generator for catalytic redox reaction, the limited studies in terms of the enzyme properties affecting signal amplification were mainly concentrated on maintaining their stability and activities. Over the past few years, several approaches involving the use of biotinylated conjugates to increase the number of associated streptavidin-enzyme molecules, the association of multiple enzymes, and enzyme on carriers, such as carbon nanotubes (Gao et al., 2011; Li et al., 2010; Dong et al., 2010) and gold nanoparticles (GNPs) (Wang et al., 2013), have also been reported for signal amplification. However, exaggerating

* Corresponding authors at: College of Environmental Science and Engineering, Hunan University, Changsha 410082, Hunan, PR China. Fax: +86 731 88822778.
E-mail addresses: tanglin@hnu.edu.cn (L. Tang), zgming@hnu.edu.cn (G. Zeng).

http://dx.doi.org/10.1016/j.bios.2014.10.063
0956-5663/

enzyme itself and scaffolded-gold nanoclusters were seldom reported.

Recently, metal nanoclusters (NCs) constitute a new class of material that has been intensively pursued. NCs are highly attractive for biolabeling and bioimaging applications because of their ultrafine size and nontoxicity (Xie et al., 2009). Among the precious metals, gold nanoclusters (GNCs) have received extensive attention because of their interesting optical properties (Zhu et al., 2008), magnetism (Negishi et al., 2006), fluorescence and electron emissions (Wen et al., 2011; Sakamoto et al., 2009), and redox properties (Sakamoto et al., 2009) as well as their potential applications in fields such as catalysis (Zhu et al., 2010a, 2010b) and optics (Liu et al., 2010; Chen et al., 2011; Shunichi et al., 2010). In fact, a myriad of different scaffolds have been used with GNCs, such as biological compounds (e.g.,DNA, proteins) (Wen et al., 2011; Chen et al., 2011) and organic compounds (Shunichi et al., 2010). However, the potential impact of this framework on enzyme catalytic role was never reported. Here, we chose a streptavidin-horseradish peroxidase (SA-HRP) scaffold for producing GNCs. SA-HRP scaffolded GNCs were successfully synthesized via a simple biomineralization process, based on the capability of a common commercially available protein, SA-HRP, Gold (III) chloride trihydrate ($HAuCl_4 \cdot 3H_2O$, 99.9%), and ascorbic acid (AA). Moreover, using enzyme-scaffolded GNCs couple with the process of electrochemical sensor assembly has rarely been reported.

On the other hand, the electrocatalytic properties of electrochemical sensor, such as sensitivity, stability and using life, are strongly related to the microstructure, surface chemistry of the electrode and the construction of electron transfer layers (Dong et al., 2012). Nanomaterials can facilitate bimolecular binding as well as accelerate electron transfer, and thus amplify electrochemical detection signal (Kang et al., 2009). In our earlier studies, we have demonstrated new strategies to increase the sensitivity and lower the detection limit of the electrochemical biosensors by using Ordered Mesoporous Carbon Nitride (MCN) as the platform for enzyme immobilization (Zhou et al., 2014). The strategy has been based on the higher affinity for bioactivator, larger bioactivity after entrapment procedure because of the CN matrix, and faster electron transfer between bioactivator and MCN-sensing sites because of the π–π* electronic transition in the MCN. These properties of MCN provide an excellent platform for bioactivator (DNA, enzyme and protein) immobilizations and faster electron transfer as well. The early uses of structurally unique structures and functional reagents have well enabled the as-prepared electrochemical biosensors to be sensitive with a low detection limit. Herein, based on our previous efforts, MCN was synthesized, then, applied to fix DNA through Au nanoparticle (GNPs) films, as a transducer to convert the recognition information into a detectable signal. Au nanoparticle (GNPs) was employed as a transducer to amplify the detectable signal, which can also couple the sulfhydryl group to easily (Tang et al., 2013) and directly immobilize mercapto biomolecules with no modifying materials. In addition to nanomaterials, a biopolymer, L-cysteine (L-Cys) has also been extensively used in biosensors due to its non-toxicity, biocompatibility, and good film-forming ability (Devi et al., 2013).

Besides, to investigate the biosensor performance, the manganese peroxidase (*MnP*) gene was used as the analyte. *MnP* is an extracellular heme-containing enzyme which can oxidize phenolic lignin model compounds and non-phenolic aromatics via radical intermediates (Li et al., 2011). As we know, lignin is a universal and recalcitrant biomaterial in agricultural and municipal solid waste. The *MnP* produced by *Phanerochaetechrysosporium*, may play a significant role in an extracellular pathway in fungal lignin mineralization (Hildén et al., 2000). In this regard, with the increasing application of composting technology in disposal of municipal solid waste, detection of *MnP* gene is of great significance to control the composting process.

This paper described an electrochemical DNA sensor using SA-HRP-scaffolded-GNCs, MCN and a biotinylated detection probe, specific to *P. chrysosporium MnP* genes on a modified electrode. It is observed in our current study that the SA-HRP-scaffolded-GNCs can exaggerate enzyme activities for the catalytic redox process, resulting in signal amplification, the relatively low detection limit and high sensitivity. The PCR amplified *MnP* fragment from *P. chrysosporium* genomic DNA was applied to the DNA sensor detection after a digestion step by restriction endonucleases with results in good agreement with the reference values deduced from electrophoresis and UV spectrometry.

2. Materials and methods

2.1. Chemicals and reagents

Pluronic copolymer P123 (EO20PO70EO20, EO=ethylene oxide, PO=propylene oxide), Tris(hydroxymethyl) aminomethane, were purchased from Sigma-Aldrich (USA). The DNA target-specific probes used for hybridization in our experiment were synthesized by Sangon (Shanghai, China) and purified using high-performance liquid chromatography. They were designed by Primer Premier 5.0 in our lab (Li et al., 2011). And the sequences of the oligonucleotides include:

5′–HS–$(CH_2)_6$–CTGATGGTGTCGTGTTTCT–3′ (M1, Capture probe of *MnP*),

5′–GATGCCGTTGTTGGCGGAGAA–biotin–3′ (M2, Detection probe of *MnP*),

5′–TTCTCCGCCAA-CAACGGCATCTTTTTTTTTTTTTTTTTTTTTTTTTTTTTTTTTTTAGAAACA CGACACCATCAG–3′ (M3, Target oligonucleotide of *MnP*),

5′–TTCTCCTCCAA-CAACGGCATCTTTTTTTTTTTTTTTTTTTTTTTTTTTTTTTTTTTAGAAACA CCACACCATCAG–3′ (M4, Two–base–mismatched oligonucleotide of *MnP*),

5′–TTCTCCTCCAACAACGGCATCTTTTTTTTTTTTTTTTTTTTTTTTTTTTTTTTTTTTTTTTAGAAACA CGACACCATCAG–3′ (M5, Single-base-mismatched oligonucleotide of *MnP*)

2.2. Preparation of MCN and assembly of SA-HRP scaffolded GNCs

The mesostructured SBA-15 silica template and MCN were synthesized as described previously in our laboratory (Zhou et al., 2014; Tang et al., 2013). Herein, we reported a simple synthetic route, based on the capability of a common commercially available protein, SA-HRP, Gold (III) chloride trihydrate ($HAuCl_4 \cdot 3H_2O$, 99.9%), and ascorbic acid (AA). It is generally agreed that this formation involved initial electrostatic attraction between Au^{3+} and negatively charged residues, followed by reduction, growth and passivation within the polypeptide chain by covalent binding (Au–S interactions) (Volden et al., 2012; Berti and Burley, 2008; Feldheim and Eaton, 2007). Here, we showed that upon adding Au (III) ions to the aqueous SA-HRP solution, the SA-HRP molecules sequestered Au ions and entrapped them (Scheme 1). Details on the procedures can be found in Supplementary information.

2.3. Electrode synthesis

Highly sensitive electrochemical DNA biosensor modified by MCN/GNPs and L-cysteine for recognition of the target sequence of *MnP* genes from *P. chrysosporium* was prepared as shown in Scheme 2. As illustrated in Scheme 2, the sensing platform was a combination of

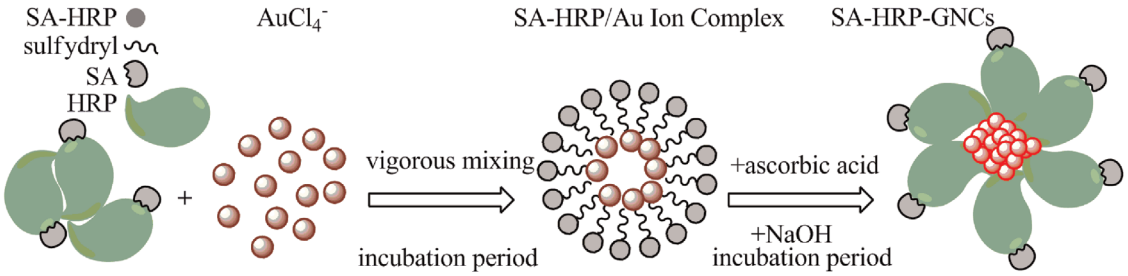

Scheme 1. Schematic of the formation of gold nanoclusters in SA–HRP solution.

MCN and GNPs film that acted as a transducer to convert the recognition information into a detectable signal. Initially, the L-Cys film modified electrode was obtained in L-Cys electrodeposition process. Then, the MCN functionalized with amino (Fig. S-1) could be covalently attached to the electrode surface through carboxyl–amino bonding. Next, the Au nanoparticles (GNPs) film modified electrode was obtained as described previously in our laboratory (Tang et al., 2013) by electrodeposition process using Gold (III) chloride trihydrate (Fig. S-2). Subsequently, the mixture solution of 10 μL capture probe was dropped onto the electrode surface and kept at 4 °C for self assembling through thiol-gold bonding for 10 h.

2.4. Detection process

The hybridization and electrochemical detection of the DNA biosensor are as follows. The modified electrode with capture

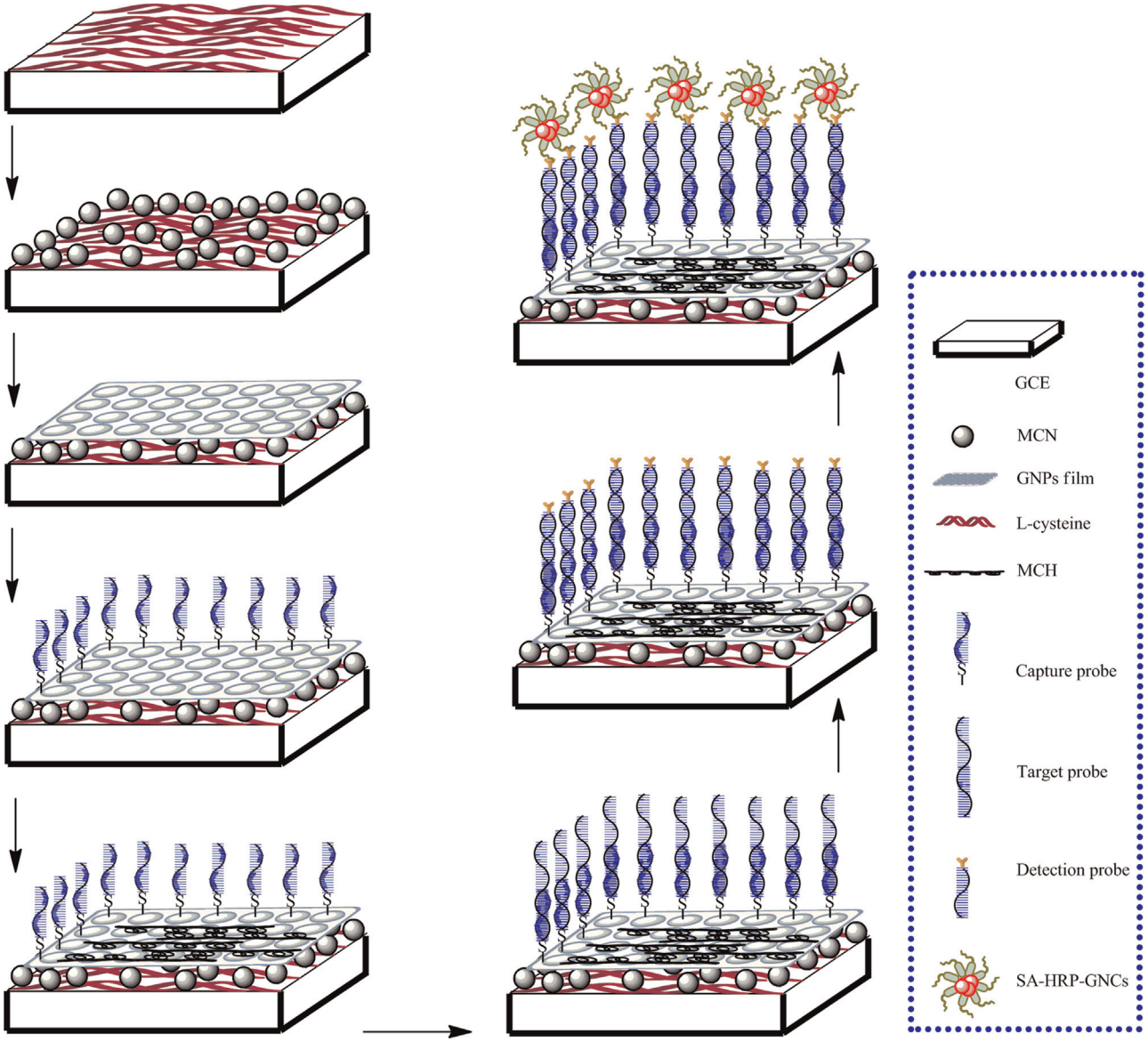

Scheme 2. A self-assembly method of this sensor.

probes coated was immersed into 400 μL of 1 mM 6-mercapto-1-hexanol (MCH) solution for 1 h to improve the quality and stability. Then, the electrode was soaked in various concentrations of target solution (200 μL) and incubated at room temperature for 1 h, and then thoroughly washed with Tris–HCl buffer. Next, the hybridization reaction was carried out by dropping 5 μL of the detection probe solution to the biosensor and incubated at room temperature for 1 h. After the biosensor was washed thoroughly with Tris–HCl buffer, 5.0 μL SA-HRP-scaffolded-GNCs was dropped on its surface, which was left for 45 min and washed Tris–HCl buffer to remove the unbound SA-HRP scaffolded GNCs. As a result, the end biotin on detection probe was "activated" by a force away from the electrode for easy access to the detection probe (Gao et al., 2011), then SA-HRP-scaffolded-GNCs is attached to biotinylated detection probe leading to a significantly amplified current signal. The electrochemical redox current catalyzed was measured using different pulse voltammetric (DPV) by the addition of 0.50 mM H_2O_2 into PBS (pH 7.38) containing 1.0 mM of hydroquinone. And the DPV measurements were performed from −200 to 600 mV with pulse amplitude of 50 mV and width of 50 s. The data for condition optimization and the calibration curve were the average values of three measurements.

2.5. MnP gene fragment preparation

The *MnP* genes fragments from *P. chrysosporium* genomic DNA were successfully extracted on potato dextrose agar (PDA) and in potato dextrose liquid medium according to the method described previously in our laboratory (Li et al., 2011; Tang et al., 2009). Proteinase K, muramidase and cetyltrimethyl ammonium bromide (CTAB) were used in the extraction process. PCR amplification and restriction-enzyme digestion were performed to obtain the target *MnP* genes fragment for the direct hybridization detection. Details on the procedures of bacteria culture, gene extraction, PCR amplification and restriction-enzyme digestion can be found in Supplementary information.

3. Results and discussion

3.1. Characterization of MNC and SA-HRP tagged GNCs

Fig. 1 shows the SEM and TEM images of MCN, and the TEM image of SA-HRP-scaffolded-GNCs. As seen in Fig. 1A, MCN was seems like chain structure. The morphological and structural studies of MCN nanoparticles were performed by TEM. Fig. 1B clearly shows a hexagonal arrangement of the mesopores. When viewed down the direction of only a stripe pattern detected, bright contrast strips on the under-focused image represented images of the pore walls, whereas dark contrast cores represented empty channels. In addition, it is seen that aggregates of SA-HRP appear as dark gray background and the encapsulated GNCs as small black dots were observed in the same area (Fig. 1C). Furthermore, it is also seen that the formation of GNCs from Fig. 1C. The TEM resolution was obscured by the enveloping protein, and thus accurate size distribution data cannot be obtained. A few big black dots were also observed in Fig. 1C. Generally, the specific ligands in the SA-HRP scaffold, especially thiol ligands, interact strongly with the noble metal surface to form ultra-fine-sized metal nanoparticles, which were protected by a monolayer of thiol ligands to form stable NCs (Xie et al., 2009; Wen et al., 2011; Nam et al., 2003). However, some small gold nanoparticles were formed in the SA-HRP scaffold aggregated during the GNCs assembly, and grew into one big particle when more entrapped Au ions were reduced on their surfaces. The in situ aggregation and growth of gold nanoparticles usually happened in further reduction process. Under the selected reduction time and conditions according to references (Wen et al., 2011; Xie et al., 2009), the majority of the gold nanoparticles could be kept small in the SA-HRP scaffold. The Fourier transform infrared (FT-IR) spectra, nitrogen adsorption–desorption isotherms and pore size distribution (inset) of SBA-15 and MCN were presented in Fig. S-3 in Supplementary information, and the results were described in Supplementary information. Besides, the formation of SA-HRP-scaffolded-GNCs label was confirmed by UV–visible spectroscopy and Mastersizer 2000 (Fig. S-4 and S-5), and the results were also described in Supplementary information.

3.2. Characterization of electrode assembly process

To test the performance of the modified electrode, CV and electrochemical impedance spectroscopy (EIS) were carried out in phosphate buffer (pH 7.38) containing 5 mM $[Fe(CN)_6]^{3-/4-}$ (1:1) and 10 mM KCl. As seen in Fig. S-6A, the immobilization of L-Cys on the GCE led to a significant decrease in peak current of the redox probe. After modification with MCN and GNCs, the peak current increased obviously and the peak potential difference reached the minimum. Following self-assembly of the DNA probe, the peak current decreased slightly and the peak potential difference grew appreciably, indicating that the modified electrode had a good current response capability.

Correspondingly, electrochemical impedance spectroscopy (EIS) of $[Fe(CN)_6]^{3-/4-}$ can provide information about the impedance changes of the electrode surface during the modification process. The interface can be modeled by an equivalent circuit. This equivalent circuit includes the electron-transfer resistance (R_{CT}), the warburg impedance (Z_w), the ohmic resistance of the electrolyte (R_s), and interfacial capacitance (C_{dl}). EIS includes a

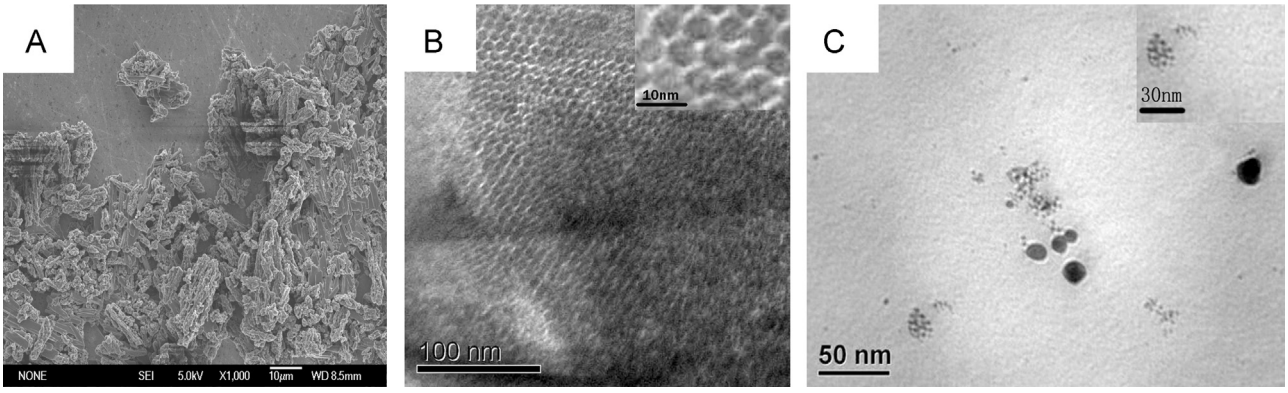

Fig. 1. (A) SEM image of MCN. (B) TEM image of MCN. (C) TEM image of SA-HRP-scaffolded-GNCs.

semicircular part and a linear part. The semicircle diameter could represent the electron-transfer resistance, R_{CT}, which dominates the electron transfer kinetics of the redox probe at the electrode interface. Meanwhile, the linear part at lower frequencies corresponds to the diffusion process. As seen in Fig. S-7, the good agreement between the measured data and the fitting curve indicates that this equivalent circuit (Fig. S-8A) is suitable and meaningful for this electrochemical system. Therefore, this equivalent circuit is used to fit the impedance spectroscopy data and extract the values of the equivalent circuit elements (Table S-1).

An almost straight line was observed for the assembly of MCN and GNPs on the modified GCE (Fig. S-6B), and the values of R_{CT} were 61.5 Ω and 58.6 Ω (Table S-1), indicating that the introduction of MCN and GNPs could improve the electron transfer kinetic to a large extent. Moreover, an obvious increase in the interfacial resistance was observed when L-Cys and DNA were entrapped in the modified electrode (Fig. S-6B). The value of R_{CT} was increased to 1351.0 Ω and 745.9 Ω, respectively (Table S-1). Such increased R_{CT} could be ascribed to the low conductivity of L-Cys and DNA, which slowed down the redox reaction of $[Fe(CN)_6]^{3-/4-}$. Although the L-Cys film does not increase electrical conductivity, the rate of electron transfer, also does not have catalytic effect in the process of the construction of the biosensor, it can make the MCN film then GNPs film more tightly through carboxyl. This method may extend the using life and stability of the biosensor. What's more, the electron transfer ability reflected by changes in the impedance of the modified electrode was in accordance with the current response reflected by cyclic voltammetry (Fig. S-6A).

As seen in Fig. S-9, it could confirm that the value of current was very small after hybridization without the target probe and detection probe, and finally, shifted back after adding detection probe. This result should be due to the fact that the immobilized detection probe was in the "closed" state in the absence of the target, which shielded biotin from being approached by the SA-HRP-scaffolded-GNCs bioconjugate due to the steric effect. And the small response resulted from the nonenzymatic reduction of H_2O_2 or nonspecific adsorption of a small amount of SA-HRP-scaffolded-GNCs on the sensor.

3.3. Catalytic reaction mechanism of biosensor

Horseradish peroxidase (HRP) is a glycolprotein containing a single protohemin in its active site (Zatón and OchoadeAspuru, 1995)). It carries out one-electron oxidation on hydroquinone and single two-electron catalysis on H_2O_2 as substrate. The following three steps describe the redox process of hydroquinone catalyzed by HRP. The first step involves the two-electron oxidation of the ferriheme prosthetic group of the peroxidase by H_2O_2. This reaction results in the formation of an intermediate, HRP (I) (oxidation state +4), consisting of oxyferryl iron (Fe (IV) 0=O) and a porphyrin ð cation radical. In the second step, the porphyrin radicalcation of HRP (I) is reduced by the one-electron donor hydroquinone (HQ) to yield the HRP (II) and the hydroquinone cation radical (Q) (Li et al., 2011; Tang et al., 2005). The later in turn accepts an additional electron from the second donor molecule hydroquinone in the third step, whereby the enzyme is returned to its native resting state, ferriperoxidase. The electrode current was found due to an electrochemical reduction of HRP (I) and HRP (II). The reaction equations are described as follows:

$$HRP\ (Fe^{3+}) + H_2O_2 \rightarrow HRP\ (I) + H_2O$$

$$HRP\ (I) + HQ \rightarrow HRP\ (II) + Q$$

$$HRP\ (II) + HQ \rightarrow HRP\ (Fe^{3+}) + Q + H_2O$$

$$Q + 2e + 2H^{+} \rightarrow HQ$$

As seen in Fig. 2A, the detection solution exhibited a stable DPV peak at 0.035 V (curve a), and the signal originated from SA-HRP-scaffolded-GNCs label (curve a) was 1. 66-fold larger than that from SA-HRP (curve b) as 10 pM target DNA. Besides, the signal originated from SA-HRP-scaffolded-GNCs label (curve a) was 4.10-fold larger than the background (curve c), which was detected in absence of target and detection probe, and came from the nonspecific adsorption of SA-HRP-scaffolded-GNCs. The reason might be the fact that the use of SA-HRP-scaffolded-GNCs label, resulting in signal transduction and amplification. As presented in Fig. 2B, the enzyme label made each target hybridization event related to numerous enzyme reactions, thus greatly amplifying the detection signal. In triggering step (I), $HRP(Fe^{3+})$ converts one substrate (here H_2O_2) into H_2O, and changed into $HRP(I)(Fe^{4+})$ that triggers redox cycling (I). And in redox cycling (II), HRP (I) and HRP (II) catalytically oxidized hydroquinone to 1, 4-benzoquinon (Li et al., 2011; Tang et al., 2005). In addition, this biosensor exhibits other common signal amplification through MCN, GNPs and the gold core, due to these materials had high conductivity in accelerating the electron transfer. Furthermore, GNCs might perform electrocatalysis. Protein-scaffolded-GNCs consisted of Au (0) and small amount of Au (I), and the Au (I) present on the surface of the gold

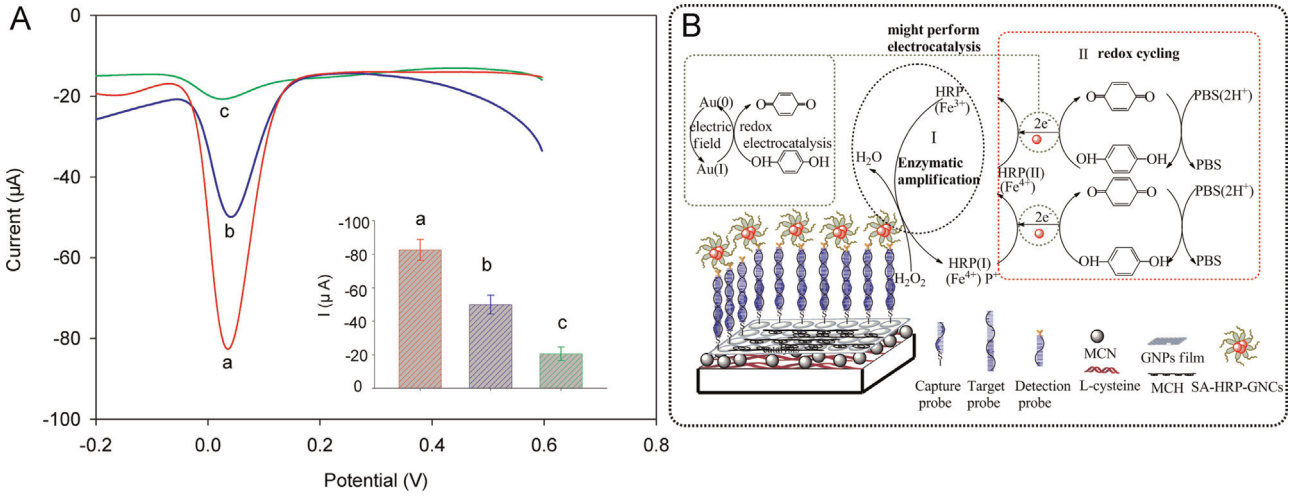

Fig. 2. (A) DPV curves of (a) 10 pM target with SA-HRP-scaffolded-GNCs, (b) 10 pM target with SA-HRP and (c) blank with SA-HRP-scaffolded-GNCs. Inset: the corresponding peak currents. Error bars indicate standard deviations from three replicative tests. (B) Enzymatic amplification and redox cycling mechanism of biosensor.

core helped to stabilize the NCs (Xie et al., 2009; Whetten and Price, 2007; Jadzinsky et al., 2007). Thus, a hypothetical reaction that might occur is the electrocatalytical reaction by Au (I) and Au (0) surface sites on the nanocluster (Girault, 2004). Namely, GNCs with the Au (I) might become a redox electrocatalyst (Brust and Gordillo, 2012; Yagi et al., 2004). Therefore, taking advantage of these signal amplification, SA-HRP-scaffolded-GNCs, GNCs, GNPs film and MCN have been successfully applied to electrochemical biosensing, resulting in a relatively low detection limit, wide linear range and high sensitivity.

3.4. Target DNA detection

Under the optimization of biosensing condition (Fig. S-10), the differential pulse voltammetric (DPV) signal was intensified in a concentration dependent manner under optimal conditions. With the increasing concentration of target DNA, the DPV peak current increased (Fig. 3). As seen in Fig. 3 (inset), the cathodic peak current was linear with the common logarithmic value of target concentration ranging from 10^{-17} M to 10^{-9} M. A linear regression equation was obtained as

$$Y = (-7.3657 \pm 0.1912)X + (-142.3142 \pm 2.5337)$$

Where Y is the current change (μA), X is the common logarithmic value of the target concentration (M), and the coefficient is 0.9946.

The detectable concentration range was relatively wide, and the sensitivity was estimated to be 6.01×10^4 A/M ($n=8$). As the current signal was three times of the standard deviation measured in blank, the limit of detection (LOD) was calculated to be 8.0×10^{-18} M. Compared to enzyme (SA-HRP)-labeled and CNTs-based sensor (Gao et al., 2011), and other enzyme-based electrochemical DNA sensors (Wang et al., 2008; Dong et al., 2012; Liu et al., 2013), the proposed biosensor exhibited improved analytical performances in terms of linear detection range, and showed a much lower detection limit. The limit of detection was also competitive with other highly sensitive detection approaches such as GaN nanowires (NWs) (Sahoo et al., 2013), and nanoparticle-based signal amplification strategy (Kwon and Bard, 2012), as presented in Table 1.

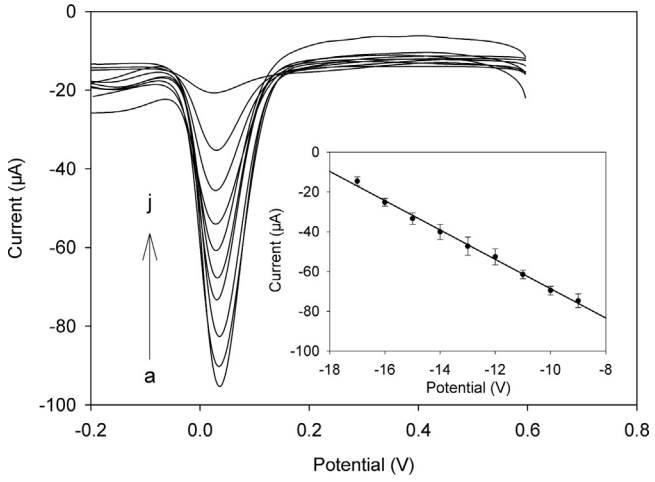

Fig. 3. DPV curves at target DNA concentrations of (a) 10^{-9} M, (b) 10^{-10} M, (d) 10^{-11} M, (d) 10^{-12} M, (e) 10^{-13} M, (f) 10^{-14} M, (g) 10^{-15} M, (h) 10^{-16} M, (i) 10^{-17} M, (j) 0 M. (a)–(j). Inset: linear relationship between peak current and common logarithm of target concentration ($n=3$).

3.5. Interference test

In order to verify the selectivity of the biosensor, the two-base mismatched response probe and single-base-mismatch sequence were used for the interference test. Under the same optimized hybridization and electrochemical conditions, the proposed DNA biosensor was investigated by exposing it to two-base-mismatched oligonucleotide and single-base-mismatch sequence at the concentration of 10 pM with three replicate measurements, respectively. The biosensor exhibited good performance to discriminate complementary target and the mismatched targets (Fig. S-11). The complementary target (Fig. S-11a) showed a signal of 3.03 fold (not minus the background value) of the two-base mismatched oligonucleotide (Fig. S-11b), and 2.36-fold of the single-base-sequence (Fig. S-11c), indicating good selectivity and great potential for the nucleotide polymorphism analysis.

3.6. Detection of MnP genes from P. chrysosporium

To evaluate the practicality of the present method, the denatured *MnP* fragment from *P. chrysosporium* genomic DNA was applied to the DNA sensor detection after PCR amplification and restriction-enzyme digestion. Gel electrophoresis analysis of extracted genomic DNA, PCR products of *MnP* gene, and digested products can be found in Supplementary information (Fig. S-12). *MnP* gene was captured on the electrode by hybridizing with the complementary capture probes (Scheme 2). The concentration of the nucleic acids directly corresponded to the electrochemical responses of SA-HRP-scaffolded-GNCs labeled on the electrode. The comparison between the detection results of *MnP* fragment samples from *P. chrysosporium* genomic DNA by the DNA sensor and UV spectrometry were shown in Table S-2. As can be seen, the recovery yield of *MnP* obtained by linear regression model ranges from 84.13% to 109.68%, and the relative standard deviation ranges from 5.49% to 12.19%. From the results, it is found that the detection result from the real sample at low concentration was not so satisfying, which might be caused by the steric hindrance since the much larger molecular size of the gene fragment (Tang et al., 2009) reduced the effective number of the immobilized capture probe available for hybridization and led to less efficient hybridization with detection probe, which then affected the immobilization of SA-HRP-scaffolded-GNCs and led to small and unstable signals.

3.7. Repeatability and reproducibility of the biosensor

The repeatability of the same biosensor (concentrations of target solution) was examined by detecting 10 pM target oligonucleotide of *MnP* in 1/15 M PBS (containing 1.0 mM of hydroquinone and 0.50 mM H_2O_2) using DPV technique (Fig. S-13), and the results were described in Supplementary information. The reproducibility was investigated with five different GCEs constructed by the same steps independently (Fig. S-14), and the results were also described in Supplementary information.

From all of these experiments, we demonstrated that the DNA sensor exhibited good precision, stability, sensitivity, and selectivity, and discriminated satisfactorily against mismatched nucleic acid samples of similar lengths, which may be ascribed to the following four factors: First, MCN/GNPs were adsorbed on the electrode surface by linking the –SH of L-Cys through thiol–gold bonding, and used as carriers for loading numerous DNA labels and accelerating electron-transfer (Fig. S-6) after an enzymatic catalytic reaction of HRP because of the π–π* electronic transition in the MCN (Girault, 2004) and it's unique electronic, chemical properties. Second, the use of low concentration L-Cys protected the link between MCN/GNPs and GCE by forming a film. They can make the MCN–GNPs film fixed more tightly through its thiol-gold

Table 1
A comparison of analytical characteristics towards DNA biosensors reported in the literature.

Electrode/enzyme	Method	Linear range (mol L^{-1})	LOD (mol L^{-1})	References
Ferrocene-Capped Gold Nanoparticle/Streptavidin conjugates modified gold electrodes	Voltammetric	11×10^{-12}–5.6×10^{-9}	2.2×10^{-12}	Wang et al., 2008
Gold electrode/SA-HRP	Chronoamperometric	6×10^{-7}–3×10^{-5}	3×10^{-8}	Tang et al., 2009
G_2-PAMAM–MWNT modified GCE	EIS	5×10^{-13}–5×10^{-10}	1×10^{-13}	Zhu et al., 2010a, 2010b
GNPs and PFG modified GCE/SA-HRP-CNTs	DPV	10^{-17}–10^{-12}	2.8×10^{-18}	Gao et al., 2011
Pt NP/Au UME	Chronoamperometric	1×10^{-11}–1×10^{-8}	—	Kwon and Bard, 2012
ERGO modified GCE/HRP	DPV	10^{-17}–10^{-13}	5×10^{-18}	Dong et al., 2012
ITO-coated glass slide	EIS	5×10^{-15}–2×10^{-12}	5×10^{-16}	Gao et al., 2013
BSA-decorated gold electrodes/HRP	Chronoamperometric	1×10^{-14}–1×10^{-8}	0.01	Liu et al., 2013
G_3-PAMAM–GaN NWs	EIS	10^{-19}–10^{-8}	—	Sahoo et al., 2013
MCN modified GCE/SA-HRP-scaffolded-GNCs	DPV	1×10^{-17}–1×10^{-9}	8.0×10^{-18}	This work

Abbreviations: CNTs: carbon nanotubes; ERGO: reduced graphene oxide; G_2-PAMAM: second-generation poly (amidoamine) dendrimer; MWNT: multi-walled carbon nanotube; ITO: indium tin oxide; BSA: bovine serum albumin; G_3-PAMAM–GaN NWsPAMAM: third generation poly (amidoamine) dendrimer; GaN NWs: GaN nanowires (NWs); UME: ultramicroelectrode.

as molecular bridge. And this method might extend the using life and stability of the biosensor. Third, the use of low concentration MCH protected the link between MCN/GNPs and DNA probe by forming a film. The film structure of MCH on the electrode surface was similar to the reported function of chitosan (Zhang et al., 2011), weakening unspecific adsorptions, strengthening the orientation of the thiolated DNA probe, and the hybridization process. Though L-Cys and MCH reduced electric conductivity, its advantages outweighed its disadvantages here. The last and the most, GNCs labeled with streptavidin-horseradish peroxidase introduced more horseradish peroxidase participating in the reaction(I) (Fig. 2B) and protected HRP intrinsic catalytic activity. What 's more, the gold nanocluster might be has electrocatalysis, thus accelerating the redox cycling.

4. Conclusions

In summary, an electrochemical DNA biosensor was constructed using SA-HRP scaffolded GNCs as label, coupling with MCN and GNPs modified electrode. The SA-HRP scaffolded GNCs provided triple signal amplification for electrochemical biosensing, while the MCN and GNPs on the biosensor surface appeared to be relatively good conductor for accelerating the electron transfer. The signal amplification strategy was introduced in detail, and produced an ultrasensitive electrochemical detection of *MnP* genes down to molar level with a relatively wide dynamic working linear range. It was also found that the biosensor exhibited good precision, stability, sensitivity, and selectivity, and discriminated satisfactorily against mismatched *MnP* genes samples of similar lengths. Besides, real samples tests confirmed the potential applicability of the biosensor for the quantification of *MnP* genes. Furthermore, the proposed approach would be attractive for genetic target analysis in bioanalytical and clinic biomedical application.

Acknowledgments

The study was financially supported by the Young TopNotch Talent Support Program of China (2012), the National Natural Science Foundation of China (51222805), the Program for New Century Excellent Talents in University from the Ministry of Education of China (NCET–11–0129), Interdisciplinary Research Project of Hunan University, China Scholarship Council (CSC) (2010843195), the Fundamental Research Funds for the Central Universities, Hunan University, and Hunan Provincial Innovation Foundation for Postgraduate (CX2009B080).

Appendix A. Supplementary material

Supplementary data associated with this article can be found in the online version at http://dx.doi.org/10.1016/j.bios.2014.10.063.

References

Berti, L., Burley, G.A., 2008. Nat. Nanotechnol 2, 81–87.
Brust, M., Gordillo, G.J., 2012. J. Am. Chem. Soc. 134, 3318–3321.
Chen, W.Y., Lan, G.Y., Chang, H.T., 2011. Anal. Chem. 83, 9450–9455.
Dong, H.F., Gao, W.C., Yan, F., Ji, H.X., Ju, H.X., 2010. Anal. Chem. 82, 5511–5517.
Dong, H.F., Zhu, Z., Ju, H.X., Yan, F., 2012. Biosens. Bioelectron 33, 228–232.
Domínguez, E., Rincón, O., Narváez, A., 2004. Anal. Chem. 76, 3132–3138.
Devi, R., Batra, B., Lata, S., Yadav, S., Pundir, C.S., 2013. Process Biochem.. 48, 242–249.
Feldheim, D.L., Eaton, B.E., 2007. Nano 3, 154–159.
Gao, W.C., Dong, H.F., Lei, J.P., Ji, H.X., Ju, H.X., 2011. Chem. Commun. 47, 5220–5222.
Gao, Z.Q., Deng, H.M., Shen, W., Ren, Y.Q., 2013. Anal. Chem. 85, 1624–1630.
Girault, H.H., 2004. EPFL Press, lausanne Switzerland, First edition, 34–41.
Hildén, L., Johansson, G., Pettersson, G., Li, J.B., Ljungquist, P., Henriksson, G., 2000. FEBS Lett. 477, 79–83.
Jadzinsky, P.D., Calero, G., Ackerson, C.J., Bushnell, D.A., Kornberg, R.D., 2007. Science 318, 430–433.
Ju, H.X., Ye, Y.K., Zhao, J.H., Zhu, Y.L., 2003. Anal. Biochem. 313, 255–261.
Kang, X.H., Wang, J., Kang, X.H., Wu, H., Aksay, I.A., Liu, J., Lin, Y.H., 2009. Biosens. Bioelectron 25, 901–905.
Kwon, S.J., Bard, A.J., 2012. J. Am. Chem. Soc. 134, 10777–10779.
Li, J.S., Deng, T., Chu, X., Yang, R.H., Jiang, J.H., Shen, G.L., Yu, R.Q., 2010. Anal. Chem. 82, 2811–2816.
Li, Z., Zeng, G.M., Tang, L., Zhang, Y., Li, Y.P., Pang, Y., Luo, J., Liu, Y.Y., 2011. Biochem. Eng. J. 55, 85–192.
Liu, G., Wan, Y., Gau, V., Zhang, J., Wang, L.H., Song, S.P., Fan, C.H., 2008. J. Am. Chem. Soc. 130, 6820–6825.
Liu, J.F., Roussel, C., Lagger, G., Tacchini, P., Girault, H.H., 2005. Anal. Chem. 77, 7687–7694.
Liu, Y.H., Li, H.N., Chen, W., Liu, A.L., Lin, X.H., 2013. Anal. Chem. 85, 273–275.
Liu, Y., Tsunoyama, H., Akita, T., Tsukuda, T., 2010. Chem. Commun. 46, 550–552.
Lubin, A.A., Hunt, B.V.S., White, R.J., Plaxco, K.W., 2009. Anal. Chem. 81, 2150–2158.
Munge, B., Liu, G.D., Collins, G., Wang, J., 2005. Anal. Chem. 77, 4662–4666.
Nam, J.M., Thaxton, C.S., Mirkin, C.A., 2003. Science 301, 1884–1886.
Negishi, Y., Tsunoyama, H., Suzuki, M., Kawamura, N., Matsushita, M.M., Maruyama, K., Sugawara, T., Yokoyama, T., Tsukuda, T., 2006. J. Am. Chem. Soc. 128, 12034–12035.
Sahoo, P., Suresh, S., Dhara, S., Saini, G., Rangarajan, S., 2013. Biosens. Bioelectron 44, 164–170.
Sakamoto, M., Tachikawa, T., Fujitsuka, M., Majima, T., 2009. J. Am. Chem. Soc. 131, 6–7.
Shunichi, F., Ryo, H., Hiroaki, K., Kei, O., 2010. J. Am. Chem. Soc. 132, 11002–11003.
Song, S.P., Liang, Z.Q., Zhang, J., Wang, L.H., Li, G.X., Fan, C.H., 2009. Angew. Chem. Int. Ed. 48, 8670–8674.
Tang, L., Zeng, G.M., Shen, G.L., Li, Y.P., Liu, C., Li, Z., Luo, J., Fan, C.Z., Yang, C.P., 2009. Biosens. Bioelectron 24, 1474–1479.
Tang, L., Zeng, G.M., Yang, Y.H., Shen, G.L., Huang, G.H., Niu, C.G., Sun, W., Li, J.B., 2005. Int. J. Environ. Anal. Chem. 85, 111–125.
Tang, L., Zhou, Y.Y., Zeng, G.M., Li, Z., Liu, Y.Y., Zhang, Y., Chen, G.Q., Yang, G.D., Lei, X. X., Wu., M.S., 2013. Analyst 138, 3552–3560.
Taton, T.A., Mirkin, C.A., Letsinger, R.L., 2000. Science 289, 1757–1760.
Volden, S., Lystvet, S.M., Halskau, W., Glomm, W.R., 2012. RSC Adv 31, 11704–11711.

Wang, J.X., Zhu, X., Tu, Q.Y., Guo, Q., Zarui, C.S., Momand, J., Sun, X.Z., Zhou, F.M., 2008. Anal. Chem. 80, 769–774.
Wang, Y.K., Yan, Y.X., Ji, W.H., Wang, H.A., Zou, Q., Sun, J.H., 2013. J. Agric. Food Chem. 61, 4250–4256.
Wen, F., Dong, Y.H., Feng, L., Wang, S., Zhang, S.C., Zhang, X.R., 2011. Anal. Chem. 83, 1193–1196.
Whetten, R.L., Price, R.C., 2007. Science 318, 407–408.
Xie, J.X., Zheng, Y.G., Ying, J.Y., 2009. J. Am. Chem. Soc. 131, 888–889.
Yagi, I., Ishida, T., Uosaki, K., 2004. Electrochem. Commun. 6, 773–779.
Ye, Y.K., Zhao, J.H., Yan, F., Zhu, Y.L., Ju, H.X., 2003. Biosens. Bioelectron 18, 1501–1508.
Zatón, A.M.L., OchoadeAspuru, E., 1995. FEBS Lett. 374, 192–194.
Zhang, Y., Pilapong, C., Guo, Y., Ling, Z.L., Cespedes, O., Quirke, P., Zhou, D.J., 2013. Anal. Chem. 85, 9238–9244.
Zhang, Y., Zeng, G.M., Tang, L., Li, Y.P., Chen, L.J., Pang, Y., Li, Z., Feng, C.L., Huang, G. H., 2011. Analyst 136, 4204–4421.
Zhu, N.N., Gao, H., Xiu, Q., Lin, Y.Q., Su, L., Mao, L.Q., 2010a. Biosens. Bioelectron 25, 1498–1503.
Zhu, M., Aikens, C.M., Hollander, F.J., Schatz, G.C., Jin, R., 2008. J. Am. Chem. Soc. 130, 5883–5885.
Zhuo, Y., Ma, M.N., Chai, Y.Q., Zhao, M., Yuan, R., 2014. Anal. Chim. Acta. 809, 47–53.
Zhu, Y., Qian, H., Jin, R., 2010b. Angew. Chem. Int. Ed. 49, 11455–11462.
Zhou, Y.Y., Tang, L., Zeng, G.M., Chen, J., Cai, Y., Zhang, Y., Yang, G.D., Liu, Y.Y., Zhang, C., Tang, W.W., 2014. Biosens. Bioelectron 61, 519–525.